Available online at www.sciencedirect.com
SCIENCE DIRECT
Journal of Colloid and Interface Science 284 (2005) 729–741
JOURNAL OF Colloid and Interface Science
www.elsevier.com/locate/jcis

Drag force on a rigid spheroidal particle in a cylinder filled with Carreau fluid

Jyh-Ping Hsu [a,*], Yu-Heng Hsieh [a], Shiojenn Tseng [b]

[a] *Department of Chemical Engineering, National Taiwan University, Taipei, Taiwan 10617, China*
[b] *Department of Mathematics, Tamkang University, Tamsui, Taipei, Taiwan 25137, China*

Received 24 March 2004; accepted 13 August 2004

Abstract

The boundary effect on the drag acting on a rigid particle is investigated by considering a spheroid on the axis of a cylinder filled with a Carreau fluid. The result of numerical simulation reveals that the ratio (drag coefficient in Carreau fluid/drag coefficient in Newtonian fluid) has a maximum as the ratio (semiaxis in radial direction/radius of cylinder) varies. The presence of a wall has the effect of enhancing the convective motion in the rear part of a particle, and therefore, the formation of wakes. The influence of the shape of a particle on the drag force acting on it can be decreased either by increasing the shear-thinning effect of the fluid or by increasing the Reynolds number. The Reynolds number at which flow separation occurs is found to increase roughly linearly with the increase in the power-law exponent of the Carreau fluid.

Keywords: Wall effect; Spheroid in cylinder; Drag correction factor; Drag coefficient; Carreau fluid; Flow separation

1. Introduction

Sedimentation is a phenomenon of both fundamental and practical significance. It is widely adopted to estimate the physical properties of an entity, or to separate entities of different nature. Previous analyses of sedimentation in the literature are ample. Brenner [1], for instance, investigated analytically the settling of a nonspherical particle in an infinite Newtonian fluid under creeping flow. The result obtained was used by Blaser [2] to evaluate the hydrodynamic force acting on an ellipsoidal particle in a linear Newtonian flow field. Chhabra [3] investigated the wall effect on the free settling of particles of various shapes in a Newtonian fluid experimentally for the case where the Reynolds number is smaller than 7. The settling of an entity, including a solid particle, bubble, or drop, both in a Newtonian fluid and in a non-Newtonian fluid, was reviewed by Clift et al. [4] and Chhabra [5]. It was pointed out that if the Reynolds number is sufficiently high, wakes are formed in the rear part of a particle, and the classic Stokes law becomes inapplicable. The behavior of a particle in a non-Newtonian fluid was studied recently by several investigators [6–11]. In a study of the sedimentation of a rigid sphere along the axis of a cylindrical tube filled with a fluid, which is of an elastic and shear-thinning nature, Navez and Walters [12] concluded that the influence of the former on the drag on the sphere is less important than that of the latter. This conclusion is consistent with that of Mena et al. [13]. Rodrigue et al. [14] investigated analytically the movement of a spherical bubble and a rigid particle in an infinite Carreau fluid under conditions of creeping flow. Shahcheraghi and Dwyer [15] analyzed the problem of the flow of an incompressible Newtonian fluid over a spherical object placed in a pipe under the condition of convective flow, taking the effect of heat transfer into account. Tripathi and Chhabra [16] calculated the drag force on a spheroid moving in a dilatant fluid in the convection-flow regime. Turian [17] and Uhlherr et al. [18] conducted the experiment of the sedimentation of a rigid sphere in a circular tube filling with an elastic shear-thinning fluid. Missirlis

* Corresponding author. Fax: +886-2-23623040.
E-mail address: jphsu@ntu.edu.tw (J.-P. Hsu).

0021-9797/$ – see front matter
doi:10.1016/j.jcis.2004.08.124

et al. [19] estimated the drag coefficient of a rigid sphere moving near the wall of a circular tube filled with a power-law shear-thinning fluid under conditions of creeping flow. Ceylan et al. [20] calculated the drag force on a rigid particle settling in a power-law fluid; the result of simulation was found to be consistent with experimental observations. Their result is applicable to Reynolds numbers up to 1000 and the parameter characterizing a power-law fluid in the range 0.5 to 1. Machač et al. [21] investigated experimentally the terminal velocity of a rigid sphere moving in a Carreau fluid in the creeping flow regime. There is an extensive literature on rigid particle motion in non-Newtonian liquids. See, for example, McKinley [22], which provides an excellent review on relevant problems. A thorough account of wall effects is also presented.

In this study, the boundary effect on the drag force acting on a rigid, nonspherical particle settling in a non-Newtonian fluid is analyzed theoretically under conditions of low to medium Reynolds number. We consider the case of a spheroid, which is capable of simulating particles of various geometries by varying its aspect ratio, and a general shear-thinning fluid described by a Carreau model.

2. Mathematical modeling

Referring to Fig. 1, we consider the settling of a rigid, spheroidal particle along the axis of a cylinder filled with a Carreau fluid. Cylindrical coordinates are adopted with their origin located on the axis of the cylinder, and r and z are respectively the radial and the axial distances. Let a and b be respectively the semiaxis in the r-direction and that in the z-direction, and let L and R be respectively the length and the radius of the cylinder. The center of the particle is located on the axis of the cylinder, and the former moves with a constant velocity $-\boldsymbol{V}$. For convenience, the particle is held fixed, and the bulk fluid moves with velocity $\boldsymbol{V}$.

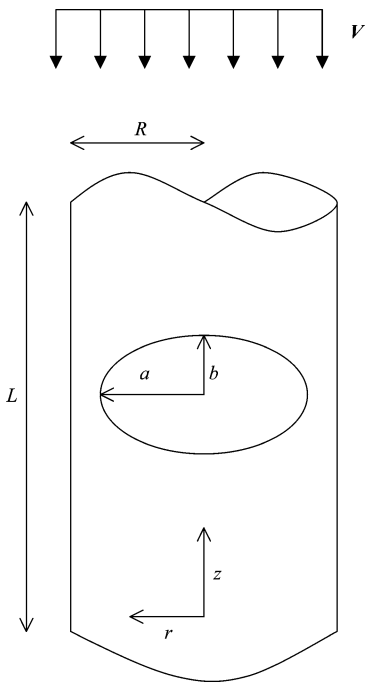

Fig. 1. Systematic representation of the problem considered. A rigid, spheroidal particle of semiaxes a and b in a cylinder of length L and radius R filled with Carreau fluid. The center of the particle is on the axis of the cylinder. r and z are respectively the radial and axial distances of the cylindrical coordinates chosen, the origin of which is located on the axis of the cylinder.

The steady-state flow field in the liquid phase can be described by the Navier–Stokes equation and the equation describing the conservation of mass,

$$\rho \boldsymbol{u} \cdot \nabla \boldsymbol{u} = -\nabla P + \nabla \cdot \boldsymbol{\tau}, \tag{1}$$

$$\nabla \cdot \boldsymbol{u} = 0, \tag{2}$$

where ρ is the density of the fluid, P is the pressure, ∇ is the gradient operator, $\boldsymbol{\tau}$ is the stress tensor, and $\boldsymbol{u}$ is the velocity of fluid. The constitutive equations for a generalized Newtonian fluid can be expressed as [5,23–25]

$$\boldsymbol{\tau} = -\eta(\dot{\gamma})\dot{\gamma}, \tag{3}$$

$$\dot{\gamma} = \nabla \boldsymbol{u} + (\nabla \boldsymbol{u})^{\mathrm{T}}. \tag{4}$$

In these expressions, $\dot{\gamma}$ and η are respectively the rate of strain tensor or shear rate and the apparent viscosity, and superscript $^{\mathrm{T}}$ denotes matrix transpose. Note that if the apparent viscosity remains constant, Eqs. (3) and (4) reduce to the constituent equations for a Newtonian fluid. For the case of a Carreau fluid [5,23–25] we have

$$\eta(\dot{\gamma}) = \eta_\infty + (\eta_0 - \eta_\infty)\left[1 + (\lambda\dot{\gamma})^2\right]^{(n-1)/2}, \tag{5}$$

where η_0 and η_∞ are respectively the viscosities corresponding to the minimum and the maximum shear rate, λ is the relaxation time constant, and n is a measure for the rate of decrease in the apparent viscosity as shear rate increases. Equation (5) describes the behavior of a shear-thinning fluid, which is one of the most important fluids exhibiting non-Newtonian behavior.

Since the particle is held fixed and the fluid moves with a relative velocity $\boldsymbol{V}$, we have the following boundary conditions for the flow field:

$$\boldsymbol{u}_z = \boldsymbol{V} \quad \text{as } r = R, \tag{6a}$$

$$\boldsymbol{u}_z = \boldsymbol{V} \quad \text{as } z \to \infty, \tag{6b}$$

$$\boldsymbol{u}_z = \boldsymbol{0} \quad \text{on particle surface.} \tag{6c}$$

The symmetric nature of the problem under consideration requires that

$$\frac{\partial \boldsymbol{u}}{\partial r} = \boldsymbol{0}, \quad r = 0, \tag{6d}$$

where $\boldsymbol{u}_z$ is the fluid velocity in the z-direction.

The governing equations, Eqs. (1)–(5), are solved numerically subject to boundary conditions, Eqs. (6a)–(6d), by FIDAP 8.6, which is based on a Gelerkin finite element

method with bilinear, four-node quadrilateral elements procedure. A total of 15,600 elements are used in the fluid domain, and the convergence criterion is 10^{-7} relative error in velocity.

The sedimentation of a particle in a fluid is often characterized by the hydrodynamic drag force it experienced, $\boldsymbol{F}$. For a rigid spherical particle of radius a moving at velocity $\boldsymbol{V}$ in an infinite Newtonian fluid, the magnitude of $\boldsymbol{F}$, F, can be expressed by [4,5,17,26]

$$F = \left(\frac{1}{2}\rho V^2\right)\left(\frac{1}{4}\pi a^2\right)C_{\mathrm{D}}, \tag{7}$$

where V is the magnitude of $\boldsymbol{V}$, ρ is the density of the fluid, and C_{D} is the drag coefficient. If V is in the creeping flow regime, C_{D} and the Reynolds number, Re, are related by the Stokes law [4,5,22,26],

$$C_{\mathrm{D}} = \frac{24}{Re}. \tag{8}$$

3. Results and discussion

The applicability of the numerical procedure adopted is justified by comparing our result with the analytical expression derived by Happel and Brenner [27] for the sedimentation of a rigid sphere along the axis of a cylinder filled with a Newtonian fluid. It was found that at $Re = 0.1$, the maximum deviation of our numerical result in the drag coefficient C_{D} from that predicted by Brenner for a/R ranges from 0 to 0.8 is smaller than 1%.

In the following discussions we assume that $\eta_\infty = 0$ poise and $\eta_0 = 2$ poise. Note that if $n = 1$ in Eq. (5), the fluid becomes Newtonian. Also, the larger the value of λ the more non-Newtonian the fluid is. For convenience, we define the Carreau number Cu as [5,23–25]

$$Cu = \frac{\lambda V}{a}. \tag{9}$$

Note that if $Cu = 0$, then the fluid is Newtonian. For the present case, the Reynolds number is defined by

$$Re = \frac{2\rho a V}{\eta_0}. \tag{10}$$

Figs. 2 and 3 illustrate respectively the contours for the shear rate and the streamlines for an oblate. Those for the case of a prolate are presented in Figs. 4 and 5. Figs. 2–5 reveals that the flow field is asymmetric at $Re = 40$ for both oblate and prolate, which is mainly due to the convective flow of fluid at the relatively large Re. Figs. 3 and 5 indicate that, due to the convective flow, wakes are formed in the rear of a particle. Figs. 2–5 also suggest that if a/R is small, that is, the particle is away from the cylinder wall, the degree of asymmetry is more serious for the case of a Newtonian fluid than for the case of the present shear-thinning fluid, but the reverse is true if a/R is large. These results imply that if the wall effect on the movement of a particle is insignificant, the shear-thinning nature of a fluid has the effect of reducing its convective motion. On the other hand, if the wall effect is important, the convective motion of a fluid is enhanced by its shear-thinning nature. Figs. 3 and 5 show that for both Newtonian and Carreau fluids the wake region in the rear of a particle at $a/R = 0.1$ is larger than that at $a/R = 0.4$ or 0.7. This is because at $a/R = 0.1$ the streamlines in the rear of a particle are more asymmetric with respect to those in front of it than at $a/R = 0.4$ or 0.7. A comparison between Figs. 3c and 3f and between Figs. 5c and 5f reveals that if a/R is large (e.g., 0.7), the shear-thinning nature of a Carreau fluid has the effect of enlarging the wake region behind a particle. Note that the streamlines in Figs. 3f and 5f are more asymmetric than those in Figs. 3c and 5c, respectively. The asymmetry of the streamlines for an oblate is more obvious than that for a prolate.

Figs. 6 and 7 show respectively the variation of the contours of viscosity for the cases of an oblate and a prolate for various a/R at two levels of Re. These figures reveal the larger Re the more asymmetric the contours are. Also, there is a drastic variation in viscosity in the rear of a particle, which implies the possibility of flow separation. This will be discussed later.

The variation of the drag coefficient C_{D} for a sphere as a function of a/R at various Carreau numbers Cu for two different Re is illustrated in Fig. 8. This figure reveals that for a fixed Cu, C_{D} increases with the increase in a/R, and for a fixed a/R, C_{D} decreases with the increase in Cu. The former is because the larger the a/R the more significant the wall effect is, and the latter is because the larger the Cu the more important the effect of shear thinning is. A comparison between Figs. 8a and 8b shows that the smaller the Re the larger the C_{D}. This is because if Re is small, the viscous force acting on a particle is more important than the inertial force acting on the particle. According to Fig. 8a, at $Re = 0.1$, C_{D} $(a/R = 0.8) = 73.56C_{\mathrm{D}}$ $(a/R = 0)$ for the case of a Newtonian fluid (i.e., $Cu = 0$). Note that $a/R = 0$ corresponds to the case where the particle is placed in an infinite fluid. If $Cu = 0.1$, then C_{D} $(a/R = 0.8) = 47.6C_{\mathrm{D}}$ $(a/R = 0)$, and if $Cu = 1$, C_{D} $(a/R = 0.8) = 22.32C_{\mathrm{D}}$ $(a/R = 0)$. That is, for a fixed nonzero a/R, C_{D} decreases with an increase in Cu. This is due to the shear-thinning nature of the fluid since the presence of wall has the effect of enhancing shear rate. According to Fig. 8b, at $a/R = 0$, C_{D} $(Cu = 1) = 0.834C_{\mathrm{D}}$ $(Cu = 0)$, which implies that the shear-thinning nature of the fluid plays a role even for the case where the wall effect is absent. This is because the shear rate at $Re = 40$ is sufficiently large to induce an appreciable decrease in the apparent viscosity of fluid. For the case $Re = 40$, C_{D} $(a/R = 0.8) = 25.8C_{\mathrm{D}}$ $(a/R = 0)$ for the case of a Newtonian fluid (i.e., $Cu = 0$). If $Cu = 0.1$, then C_{D} $(a/R = 0.8) = 17.5C_{\mathrm{D}}$ $(a/R = 0)$, and, if $Cu = 1$, C_{D} $(a/R = 0.8) = 10.05C_{\mathrm{D}}$ $(a/R = 0)$. Apparently, the increase in C_{D} due to wall effect is less appreciable than that for the case $Re = 0.1$.

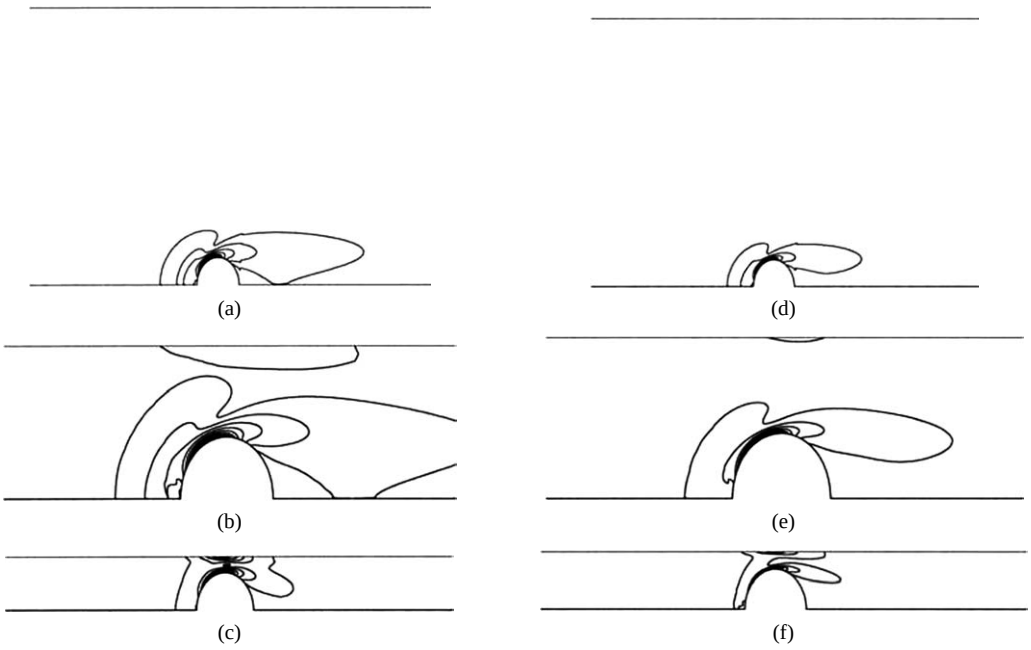

Fig. 2. Contours of shear rate for an oblate at various a/R for the case $Re = 40$, $n = 0.6$, and $a/b = 4/3$. (a) $Cu = 0$, $a/R = 0.1$; (b) $Cu = 0$, $a/R = 0.4$; (c) $Cu = 0$, $a/R = 0.7$; (d) $Cu = 1$, $a/R = 0.1$; (e) $Cu = 1$, $a/R = 0.4$; (f) $Cu = 1$, $a/R = 0.7$. Key: $a = 0.12$ cm, $\rho = 1$ g/cm^3, $\eta_0 = 2$ poise, and $\eta_\infty = 0$ poise.

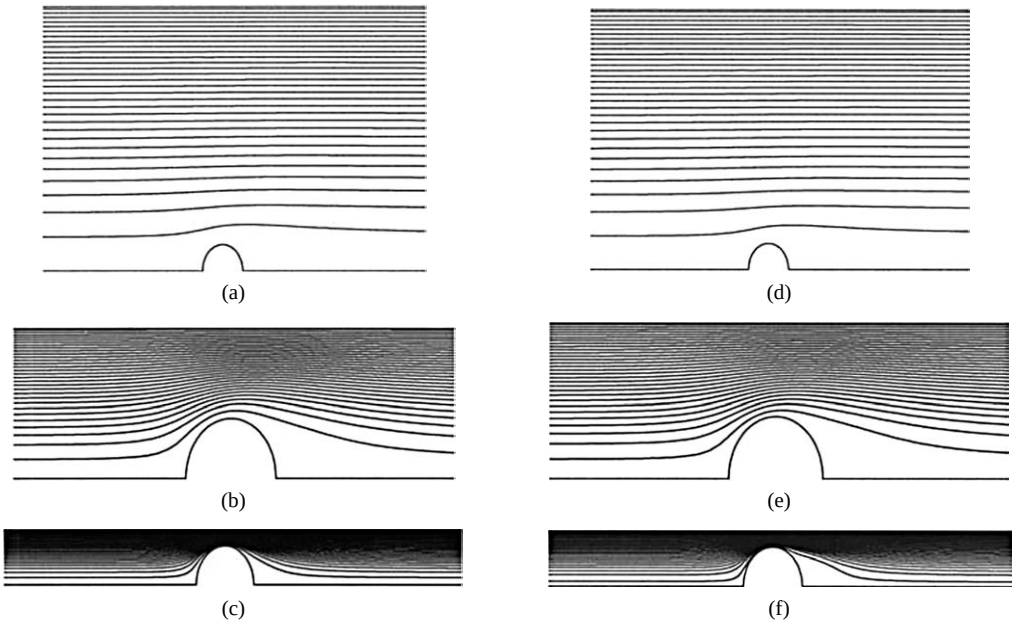

Fig. 3. Streamlines for an oblate at various a/R for the case $Re = 40$, $n = 0.6$, and $a/b = 4/3$. (a) $Cu = 0$, $a/R = 0.1$; (b) $Cu = 0$, $a/R = 0.4$; (c) $Cu = 0$, $a/R = 0.7$; (d) $Cu = 1$, $a/R = 0.1$; (e) $Cu = 1$, $a/R = 0.4$; (f) $Cu = 1$, $a/R = 0.7$. Key: same as in Fig. 2.

Fig. 9 shows the variation of the drag coefficient C_D for a prolate as a function of a/R at various Carreau numbers, Cu for two different Re, and the corresponding variation for an oblate is presented in Fig. 10. These figures reveal that the qualitative behavior of C_D for both a prolate and an oblate is the same as that for a sphere. For the case of the prolate shown in Fig. 9a, if $Cu = 0$, C_D $(a/R = 0.8) = 98.34C_D$ $(a/R = 0)$, if $Cu = 0.1$, C_D $(a/R = 0.8) = 65.45C_D$ $(a/R = 0)$, and if $Cu = 1$, C_D $(a/R = 0.8) = 29.94C_D$ $(a/R = 0)$. A comparison between Figs. 8a and 9a shows that the increase of C_D as a/R varies from 0 to 0.8 is greater for a prolate than for a sphere. This is because if a is fixed, the surface area of a prolate is greater than that of a sphere. At $a/R = 0$, if $Re = 0.1$, then C_D $(Cu = 1) \cong C_D$ $(Cu = 0)$, and if $Re = 40$, C_D $(Cu = 1) = 0.846C_D$ $(Cu = 0)$, which is slightly higher than for the case of a sphere. For the case $Re = 40$, if $Cu = 0$, C_D $(a/R = 0.8) = 34.36C_D$ $(a/R = 0)$, if $Cu = 0.1$, C_D $(a/R = 0.8) =$

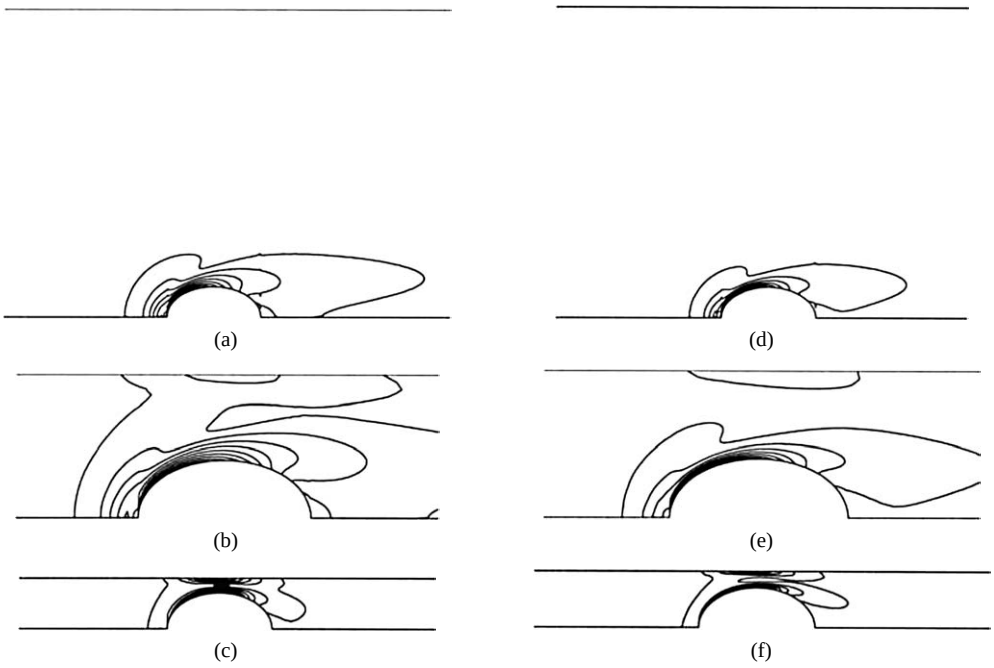

Fig. 4. Contours of shear rate for a prolate at various a/R for the case $Re = 40$, $n = 0.6$, and $a/b = 2/3$. (a) $Cu = 0$, $a/R = 0.1$; (b) $Cu = 0$, $a/R = 0.4$; (c) $Cu = 0$, $a/R = 0.7$; (d) $Cu = 1$, $a/R = 0.1$; (e) $Cu = 1$, $a/R = 0.4$; (f) $Cu = 1$, $a/R = 0.7$. Key: same as in Fig. 2.

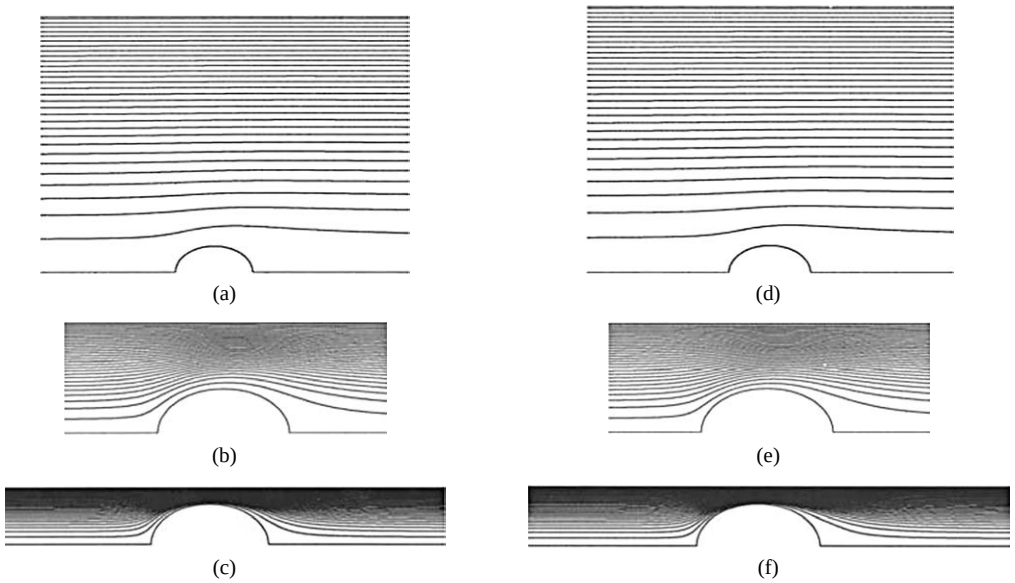

Fig. 5. Streamlines for a prolate with $a/b = 2/3$ at various a/R for the case $Re = 40$ and $n = 0.6$. (a) $Cu = 0$, $a/R = 0.1$; (b) $Cu = 0$, $a/R = 0.4$; (c) $Cu = 0$, $a/R = 0.7$; (d) $Cu = 1$, $a/R = 0.1$; (e) $Cu = 1$, $a/R = 0.4$; (f) $Cu = 1$, $a/R = 0.7$. Key: same as in Fig. 2.

$23C_D$ $(a/R = 0)$, and if $Cu = 1$, C_D $(a/R = 0.8) = 12.3C_D$ $(a/R = 0)$. As in the case of a sphere, the increase in C_D due to the variation of a/R at $Re = 40$ is smaller than that at $Re = 0.1$. The increase in C_D due to the variation of a/R is greater than that for the case of a sphere. Again, this is because for a fixed a, the surface area of a prolate is greater than that of a sphere. For the case of the oblate shown in Fig. 10 at $Re = 0.1$, if $Cu = 0$, C_D $(a/R = 0.8) = 55.3C_D$ $(a/R = 0)$, if $Cu = 0.1$, C_D $(a/R = 0.8) = 37.5C_D$ $(a/R = 0)$, and if $Cu = 1$, C_D $(a/R = 0.8) = 17.9C_D$ $(a/R = 0)$. The increase in C_D arises from the variation of a/R being smaller than that for a sphere. This is because for a fixed a the surface area of an oblate is smaller than of a sphere. At $a/R = 0$, if $Re = 0.1$, then C_D $(Cu = 1) \cong C_D$ $(Cu = 0)$, and if $Re = 40$, C_D $(Cu = 1) = 0.782C_D$ $(Cu = 0)$, which is lower than for the case of a sphere. For the case $Re = 40$, if $Cu = 0$, C_D $(a/R = 0.8) = 20.7C_D$ $(a/R = 0)$, if $Cu = 0.1$, C_D $(a/R = 0.8) = 14.38C_D$ $(a/R = 0)$, and if $Cu = 1$, C_D $(a/R = 0.8) = 9.32C_D$ $(a/R = 0)$. The increase of C_D due to the variation of a/R for an oblate is smaller than that for a sphere. Again, this is because for a fixed a the surface area of an oblate is

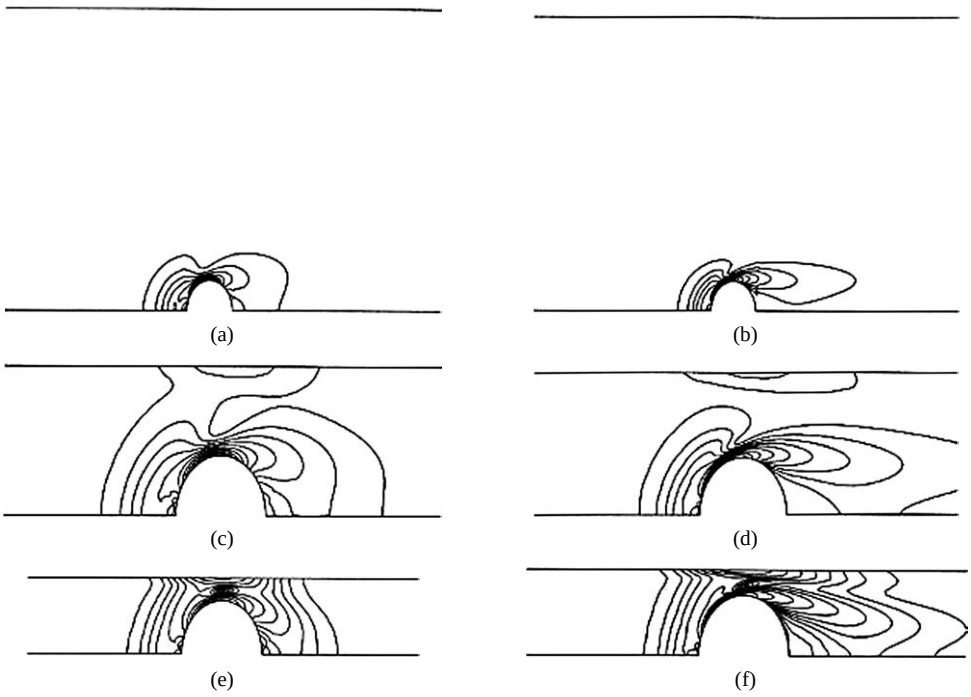

Fig. 6. Contours of viscosity for an oblate at various a/R for the case $n = 0.6$, $Cu = 1$, and $a/b = 4/3$. (a) $Re = 10$, $a/R = 0.1$; (b) $Re = 40$, $a/R = 0.1$; (c) $Re = 10$, $a/R = 0.4$; (d) $Re = 40$, $a/R = 0.4$; (e) $Re = 10$, $a/R = 0.7$; (f) $Re = 40$, $a/R = 0.7$. Key: same as in Fig. 2. Flow separation in the wake does not occur at $Re = 10$, but occurs at $Re = 40$.

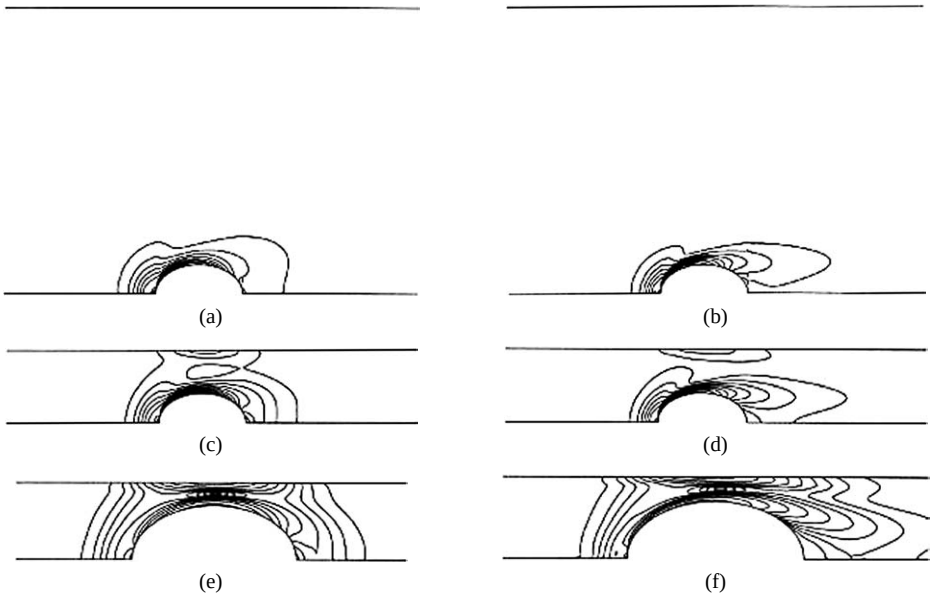

Fig. 7. Contours of viscosity for a prolate at various a/R for the case $n = 0.6$, $Cu = 1$, and $a/b = 2/3$. (a) $Re = 10$, $a/R = 0.1$; (b) $Re = 40$, $a/R = 0.1$; (c) $Re = 10$, $a/R = 0.4$; (d) $Re = 40$, $a/R = 0.4$; (e) $Re = 10$, $a/R = 0.7$; (f) $Re = 40$, $a/R = 0.7$. Key: same as in Fig. 2. Flow separation in the wake does not occur at $Re = 10$, but occurs at $Re = 40$.

smaller than that of a sphere. As in the case of a sphere or a prolate, the increase in C_D due to the variation of a/R at $Re = 40$ is smaller than that at $Re = 0.1$.

The variations of the drag coefficient C_D as a function of the Reynolds number Re for various Carreau numbers Cu and a/b at two levels of a/R are illustrated in Figs. 11 and 12. According to Eq. (8), $\log(C_D)$ and $\log(Re)$ are linearly correlated for the case of Newtonian fluid in the creeping flow regime. For the case of Fig. 11 at $Re = 40$, if $Cu = 0$ (Newtonian fluid), the deviations from the Stokes-law-like relation for a/b equal to 2/3, 1, and 4/3 are 2.2, 4.3, and 6.8%, respectively. The deviation is defined by $[(C_D - \overline{C}_D)/\overline{C}_D] \times 100\%$, where $\overline{C}_D$ is the drag coefficient based on the Stokes-law-like relation. If $Cu = 0.1$, the deviations are 2.4, 4.6, and 7.2%, respectively, and if $Cu = 1$, the deviations are 7.2, 14, and 21.4%, respectively. For the

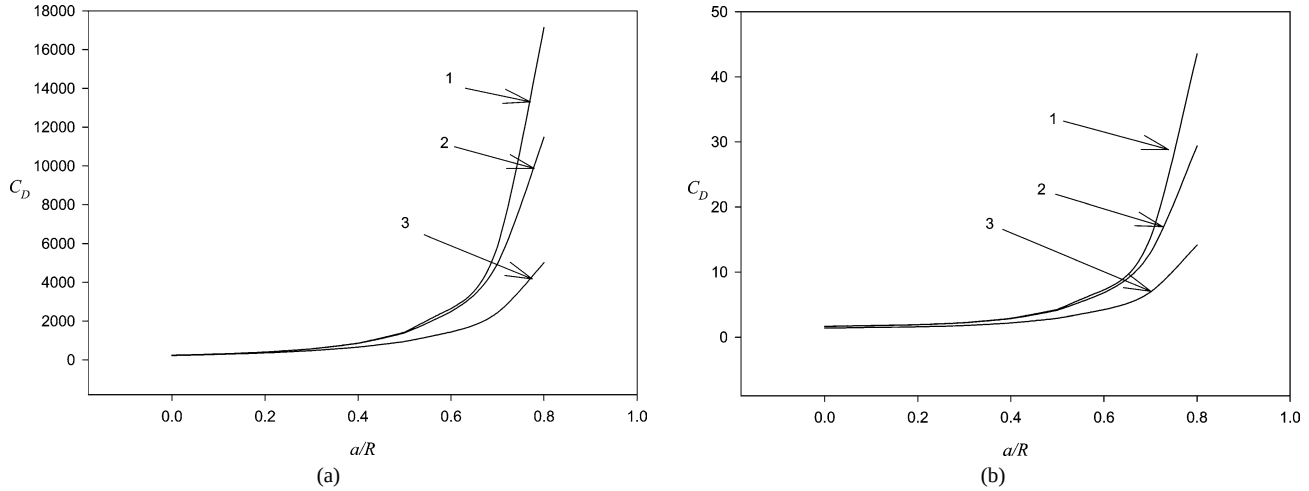

Fig. 8. Variation of C_D for a sphere as a function of a/R at various Cu for the case $n = 0.6$. Curve 1, $Cu = 0$; 2, $Cu = 0.1$; 3, $Cu = 1$. (a) $Re = 0.1$; (b) $Re = 40$. Key: same as in Fig. 2.

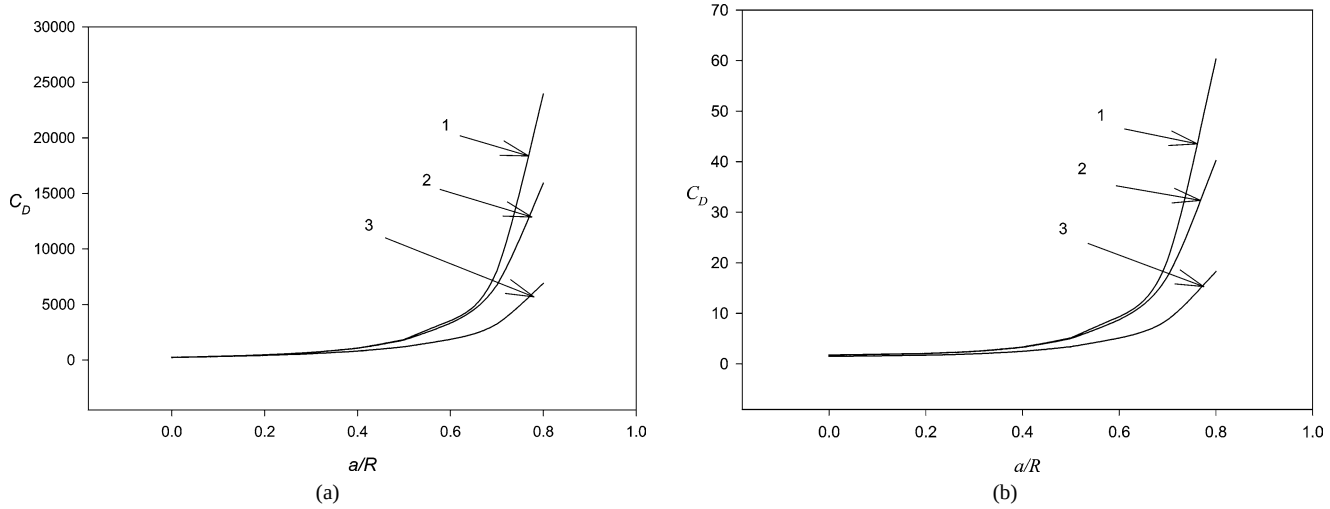

Fig. 9. Variation of C_D for a prolate as a function of a/R at various Cu for the case $n = 0.6$ and $a/b = 2/3$. Curve 1, $Cu = 0$; 2, $Cu = 0.1$; 3, $Cu = 1$. (a) $Re = 0.1$; (b) $Re = 40$. Key: same as in Fig. 2.

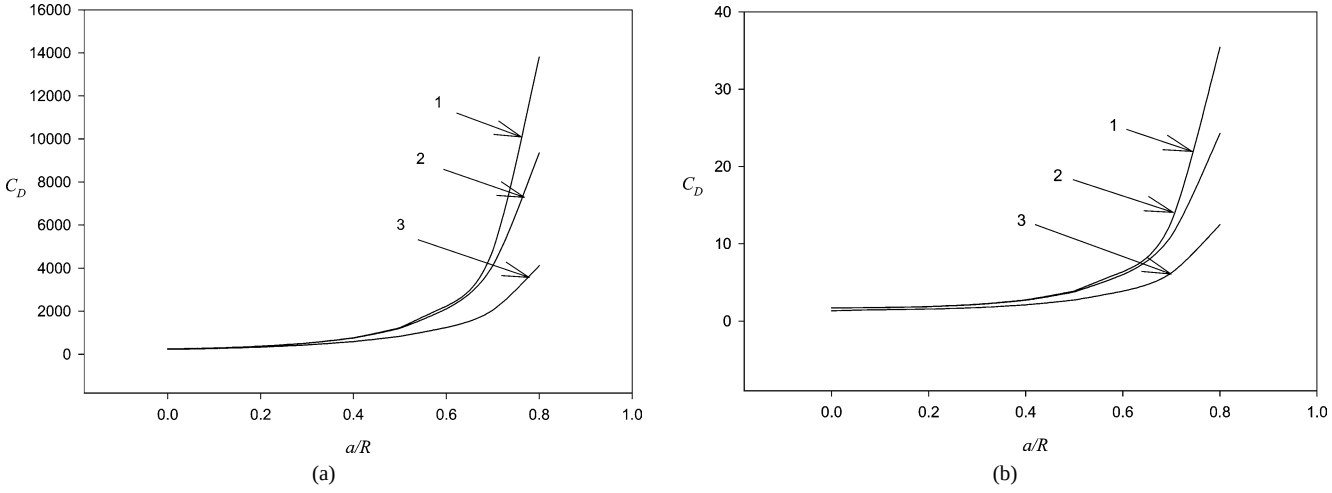

Fig. 10. Variation of C_D for an oblate as a function of a/R at various Cu for the case $n = 0.6$ and $a/b = 4/3$. Curve 1, $Cu = 0$; 2, $Cu = 0.1$; 3, $Cu = 1$. (a) $Re = 0.1$; (b) $Re = 40$. Key: same as in Fig. 2.

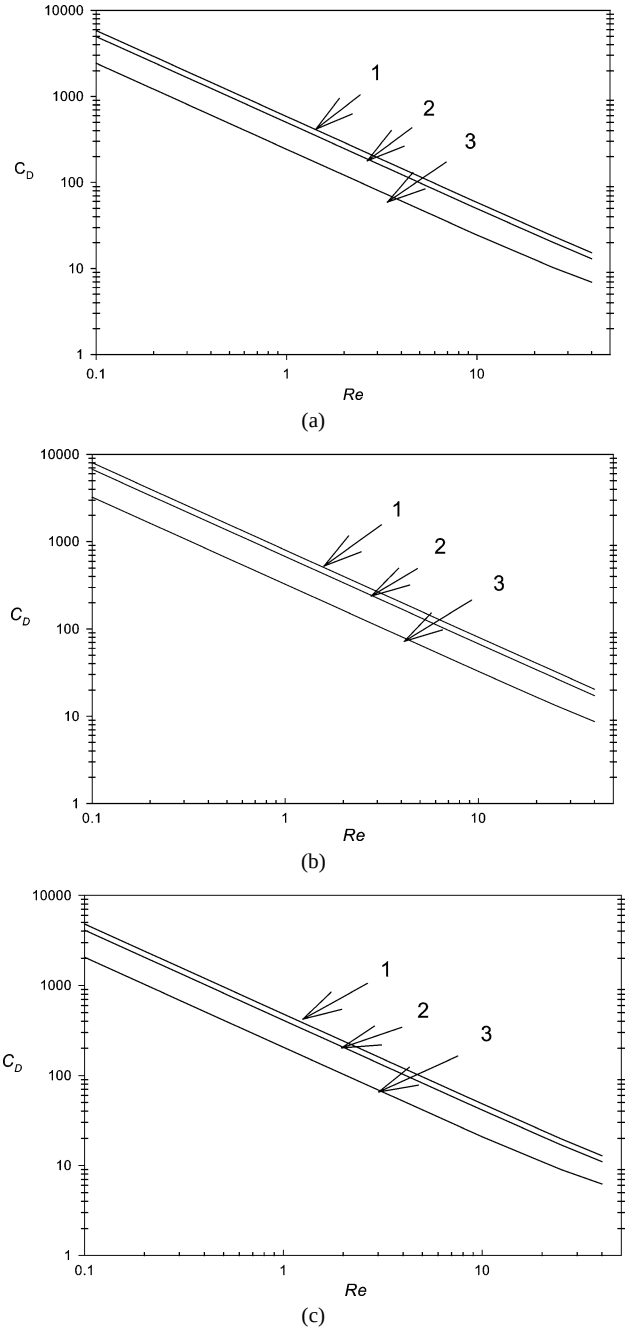

Fig. 11. Variations of C_D as a function of Re at various Cu and a/b for the case $n = 0.6$ and $a/R = 0.7$. Curve 1, $Cu = 0$; 2, $Cu = 0.1$; 3, $Cu = 1$ in both (a), (b), and (c). (a) $a/b = 1$; (b) $a/b = 2/3$; (c) $a/b = 4/3$. Key: same as in Fig. 2.

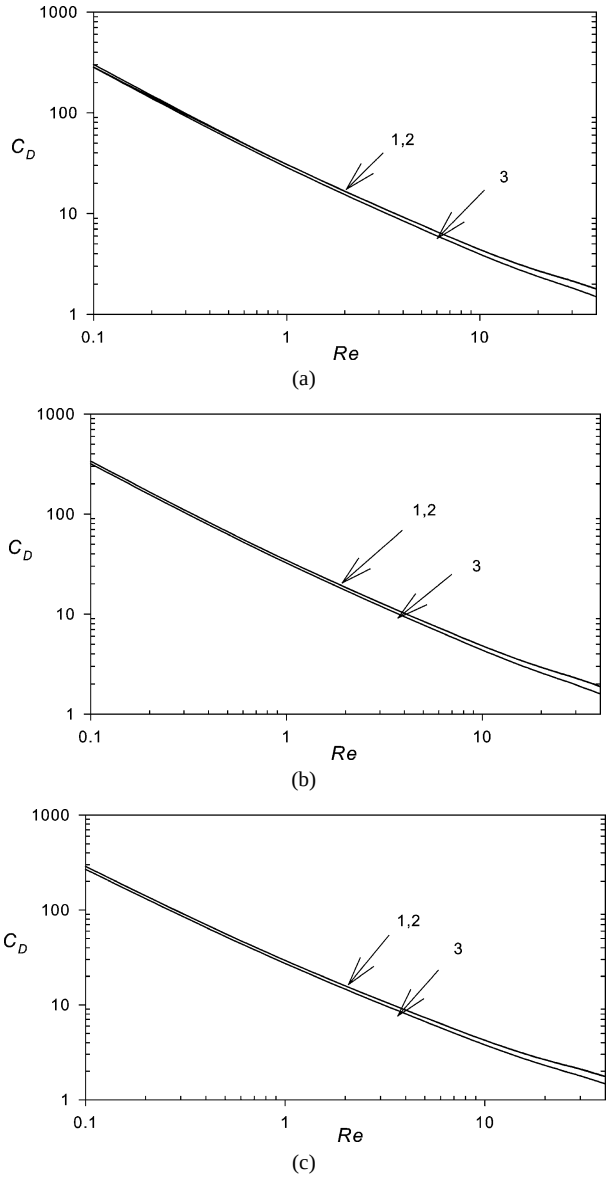

Fig. 12. Variation of C_D as a function of Re at various Cu and a/b for the case $n = 0.6$ and $a/R = 0.1$. Curve 1, $Cu = 0$; 2, $Cu = 0.1$; 3, $Cu = 1$. (a) $a/b = 1$; (b) $a/b = 2/3$, (c) $a/b = 4/3$. Key: same as in Fig. 2.

case of Fig. 12 at $Re = 40$, if $Cu = 0$ the deviations from the Stokes-law-like relation for a/b equal to $2/3$, 1, and $4/3$ are 124, 137, and 146.4%, respectively. The deviations at $Re = 40$ for $Cu = 0.1$ are almost the same as for $Cu = 0$, and the deviations for $Cu = 1$ are 101, 112, and 120%, respectively. We conclude from Figs. 11 and 12 that the shear-thinning nature of a fluid has the effect of reducing the deviation of the $\log(C_D) - \log(Re)$ relation from the Stokes-law-like relation when the wall effect is insignificant, but the reverse is true if the wall effect is significant. This conclusion is consistent with that obtained from Figs. 3 and 5.

For a sphere settling along the axis of a cylindrical tube of radius R, Navez and Walters [12] used the expression

$$F = 6\pi\eta_0 V a K, \tag{11}$$

where K is a drag-correction factor. Also, a parameter X is defined to characterize the influence of the non-Newtonian behavior of the fluid [12],

$$X = \frac{K}{K_N}, \tag{12}$$

where K and K_N are respectively the drag correction factor of a rigid particle in a shearing–thinning fluid and that of a rigid sphere in a Newtonian fluid. Both are based on

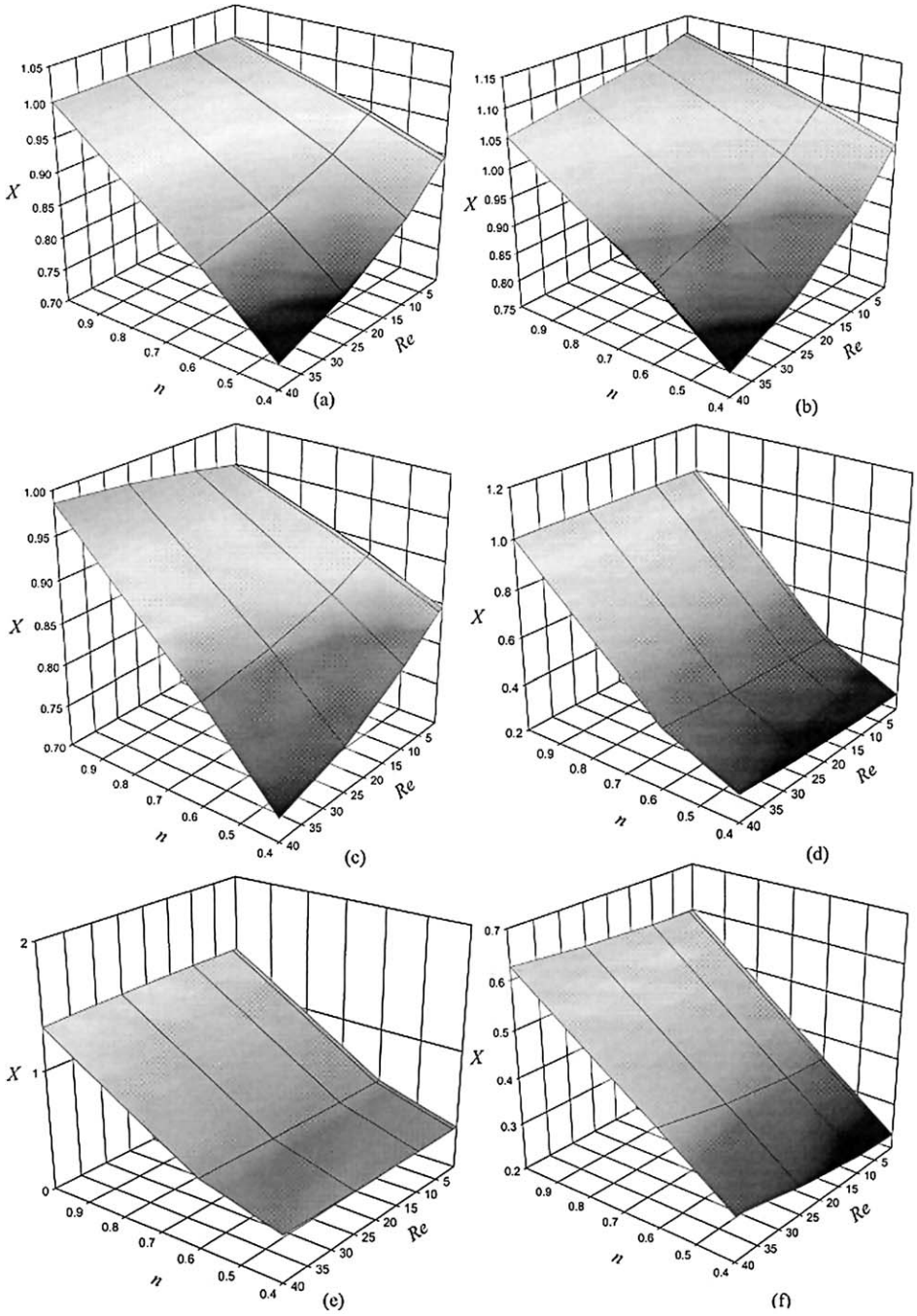

Fig. 13. Contours of X as function of Re and n at various combinations of a/b and a/R for the case when $Cu = 1$. (a) $a/b = 1$, $a/R = 0.7$; (b) $a/b = 2/3$, $a/R = 0.7$; (c) $a/b = 4/3$, $a/R = 0.7$; (d) $a/b = 1$, $a/R = 0.1$; (e) $a/b = 2/3$, $a/R = 0.1$; (f) $a/b = 4/3$, $a/R = 0.1$. Key: same as in Fig. 2.

the same a/R and Re [12]. This measure is also adopted in our study with K now representing the drag-correction factor of a rigid spheroidal in a shearing–thinning fluid. Fig. 13 illustrates the variation of X as a function of n and Re for various combinations of a/b and a/R. This figure indicates that, in general, X decreases with the decrease in n or with the increase in Re.

The variation of X as a function of a/R for the case of a prolate at various Cu for two levels of Re is shown in Fig. 14. This figure reveals that if $Cu = 0$ (Newtonian fluid), X increases monotonically with the increase in a/R. Note that for a fixed a, the surface area of a prolate is larger than the corresponding sphere, and, therefore, $X > 1$. Also, the larger the a/R, the more significant the wall effect and the larger the X. However, for the case of a shear thinning fluid, X exhibits a local maximum as a/R varies. This is because if a/R is small, the presence of a wall, which has the effect of increasing the drag force on a particle, is more significant than the shear-thinning nature of the fluid, which has the effect of reducing the drag force, and therefore X increases with the

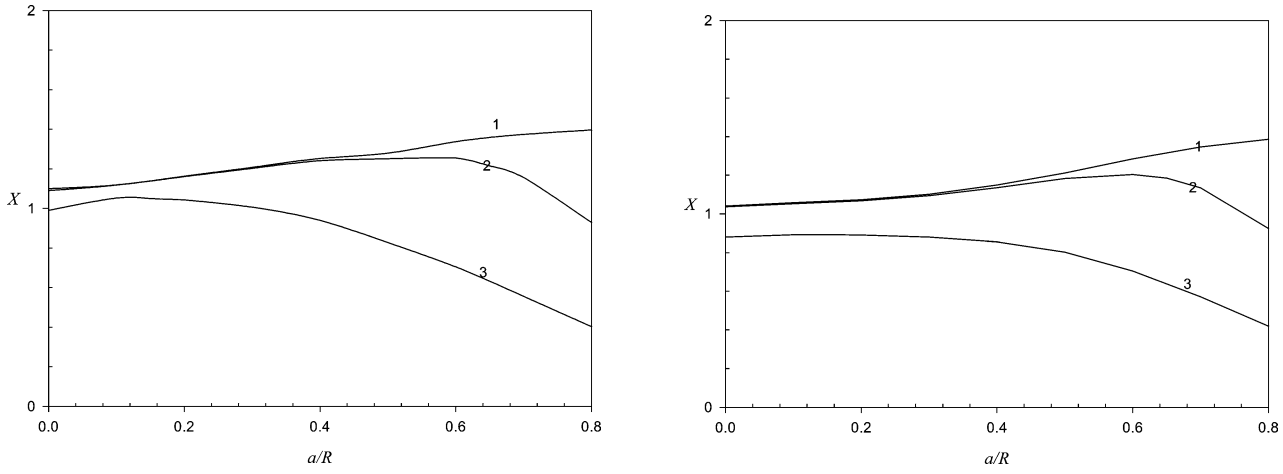

Fig. 14. Variation of X for a prolate as a function of a/R at various Cu at two levels of Re for the case $a/b = 2/3$ and $n = 0.6$. Curve 1, $Cu = 0$; 2, $Cu = 0.1$; 3, $Cu = 1$. (a) $Re = 0.1$; (b) $Re = 40$. Key: same as in Fig. 2.

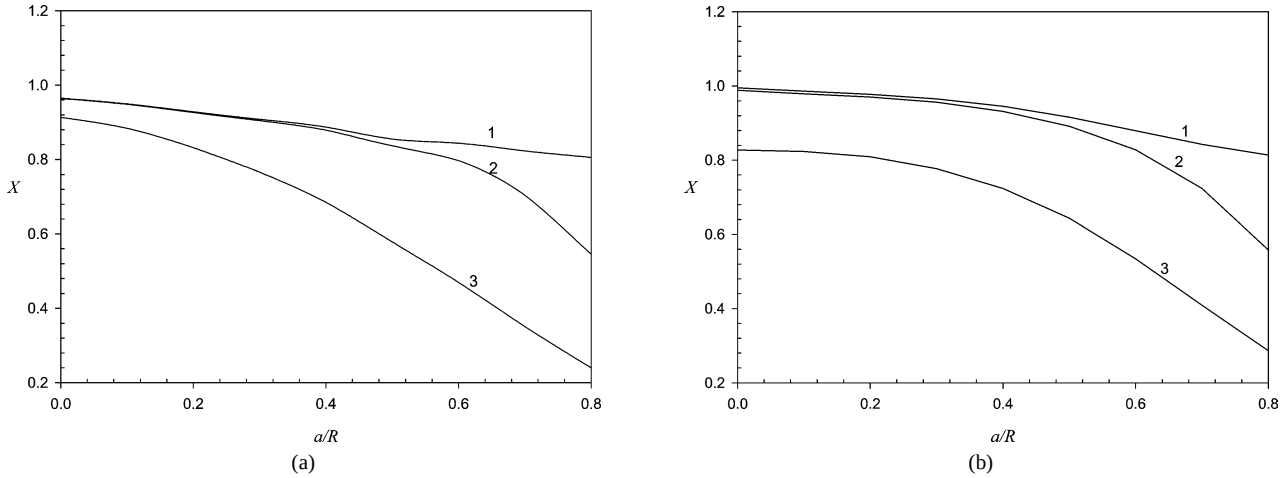

Fig. 15. Variation of X for an oblate as a function of a/R at various Cu at two levels of Re for the case $n = 0.6$ and $a/b = 4/3$. Curve 1, $Cu = 0$; 2, $Cu = 0.1$; 3, $Cu = 1$. (a) $Re = 0.1$; (b) $Re = 40$. Key: same as in Fig. 2.

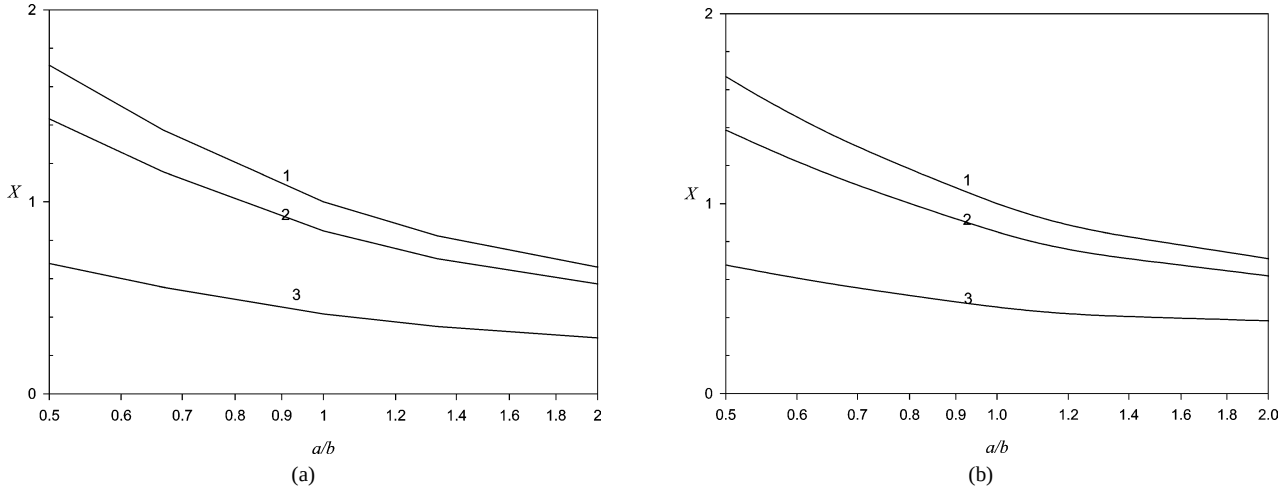

Fig. 16. Variations of X as a function of a/b at various Cu at two different Re for the case $n = 0.6$ and $a/R = 0.7$. Curve 1, $Cu = 0$; 2, $Cu = 0.1$; 3, $Cu = 1$. (a) $Re = 0.1$; (b) $Re = 40$. Key: same as in Fig. 2.

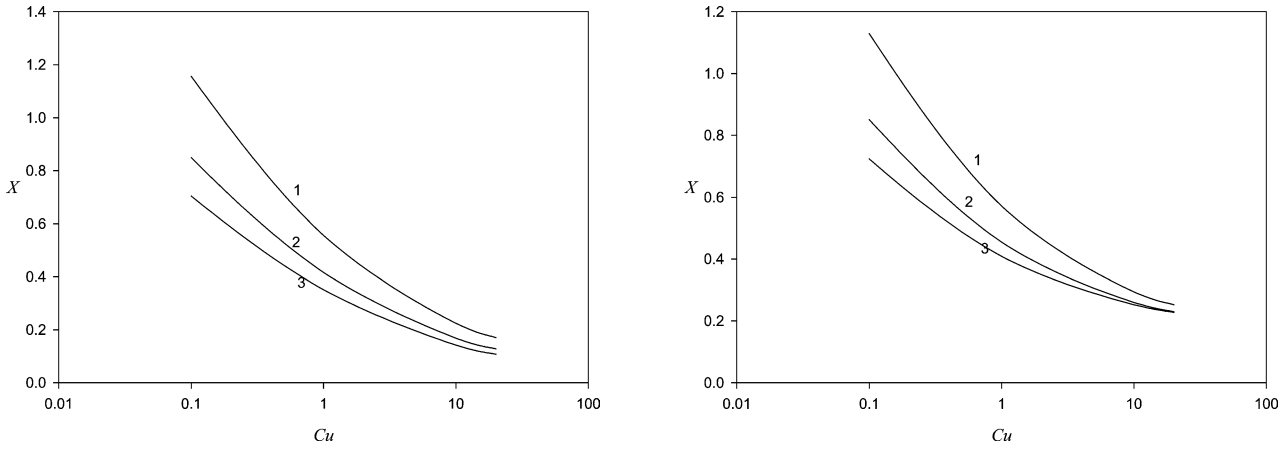

Fig. 17. Variations of X as a function of Cu at various a/b at two different Re for the case $n = 0.6$ and $a/R = 0.7$. Curve 1, $a/b = 2/3$; 2, $a/b = 1$; 3, $a/b = 4/3$. (a) $Re = 0.1$; (b) $Re = 40$. Key: same as in Fig. 2.

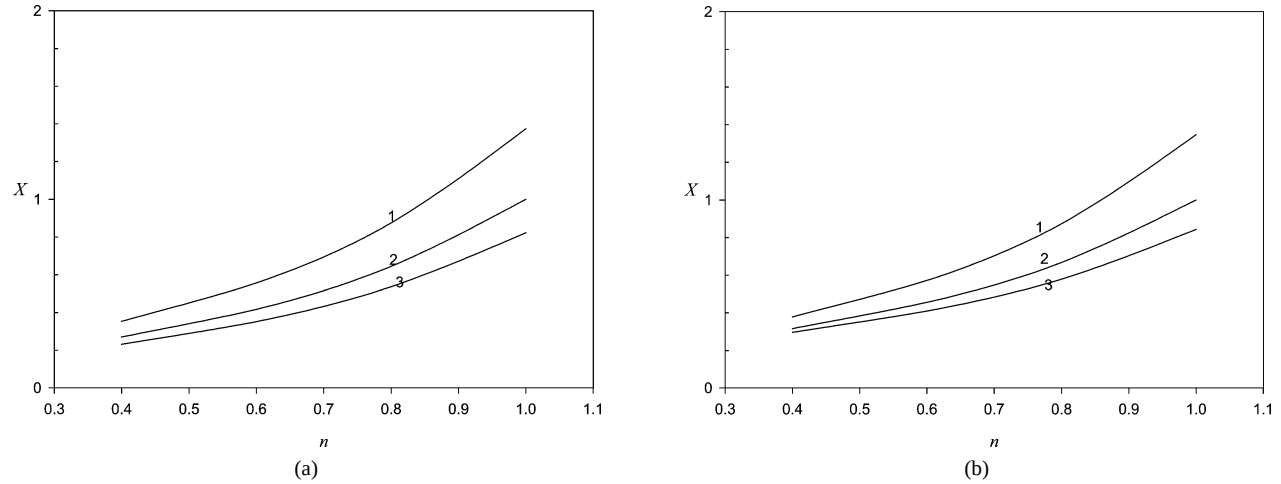

Fig. 18. Variations of X as a function of n at various a/b at two different Re for the case $Cu = 1$ and $a/R = 0.7$. Curve 1, $a/b = 2/3$; 2, $a/b = 1$; 3, $a/b = 4/3$. (a) $Re = 0.1$; (b) $Re = 40$. Key: same as in Fig. 2.

increase in a/R. On the other hand, if a/R is large, the reverse is true, and X decreases with the increase in a/R. For the case $Re = 0.1$ the maximum of X occur at $a/R \cong 0.6$ when $Cu = 0.1$, and $a/R \cong 0.15$ when $Cu = 1$; these values are about the same for the case when $Re = 40$.

The variations of X as a function of a/R for the case of an oblate at various Cu for two levels of Re are shown in Fig. 15. This figure indicates that, in contrast to the case of a prolate, if $Cu = 0$ (Newtonian fluid), X is smaller than unity and decreases monotonically with the increase in a/R. This is because the surface area of an oblate is smaller than that of the corresponding sphere. If $Cu \neq 0$, X also decreases monotonically with the increase in a/R. This is because both the presence of a wall and the shear-thinning nature of the fluid lead to smaller drag force on a particle.

The variations of X as a function of a/b for various Cu at two different Re are illustrated in Fig. 16. This figure indicates that for fixed a and Cu, X decreases with the increase in a/b. As discussed above, this is because if a is fixed, the surface area of a particle decreases with the increase in a/b. At $Re = 0.1$ and $a/R = 0.7$, X decreases 66.5, 60, and 57% as a/b varies from 0.5 to 2 for Cu equal to 0, 0.1, and 1, respectively. At $Re = 40$ and $a/R = 0.7$, X decreases 57.4, 55.3, and 43.6% as a/b varies from 0.5 to 2 for Cu equal to 0, 0.1, and 1, respectively. These imply that the influence of the shape of a particle on its X can be decreased by enhancing the shear-thinning nature of the fluid phase or by increasing the Reynolds number.

Fig. 17 shows the variations of X as a function of the Carreau number Cu for various a/b at two different Re. This figure indicates that X decreases as Cu increases, which is expected. For the case $Re = 0.1$, X decreases 85.3, 85, and 84.5% as Cu varies from 0.1 to 20 for a/b equal to 2/3, 1, and 4/3, respectively. The difference in the percentage decrease in X as Cu varies is insensitive to the shape of a particle at $Re = 0.1$. For the case $Re = 40$, X decreases 77.6, 73, and 68.5% as Cu varies from 0.1 to 20 for a/b equal to 2/3, 1, and 4/3, respectively. Apparently, the effect of the shape of a particle on the percentage decrease in X as Cu varies becomes appreciable if Re is high.

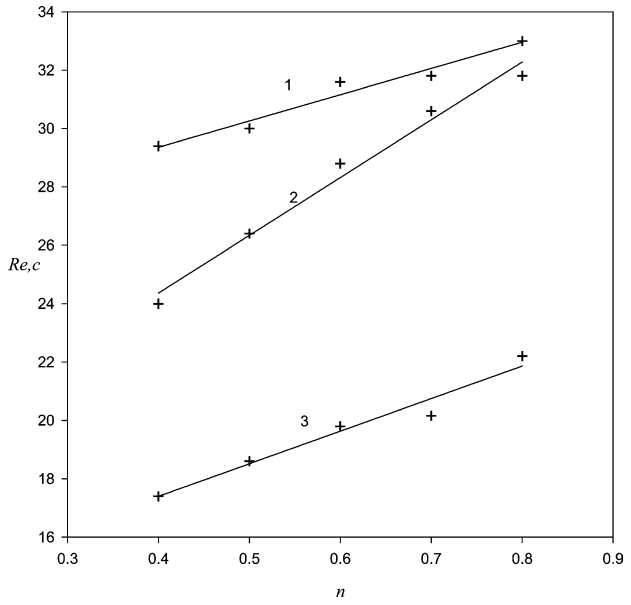

Fig. 19. Variation of critical Reynolds number, Re_c, at which flow separation in the wake occurs as a function of n at various a/b for the case $\lambda = 0.00036$ s and $a/R = 0.7$. Discrete symbols are the estimated values, and curves represent fitted results. Curve 1, $a/b = 2/3$; 2, $a/b = 1$; 3, $a/b = 4/3$. Key: same as in Fig. 2.

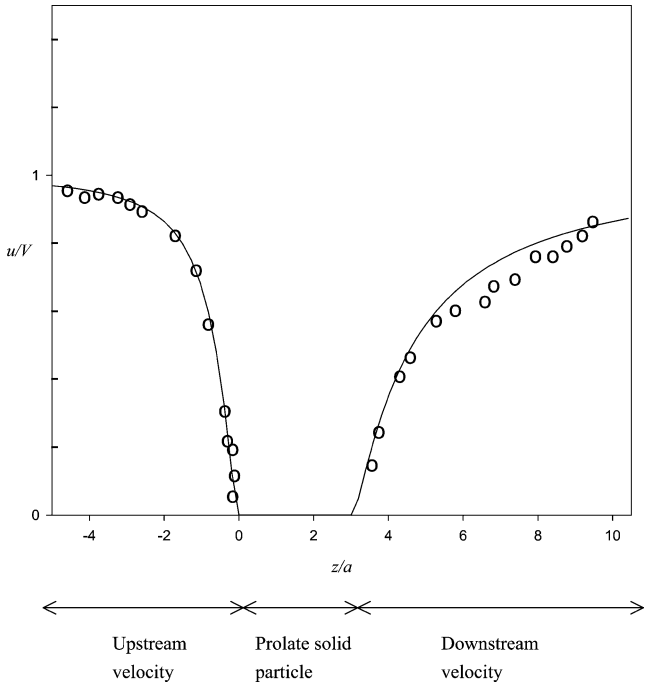

Fig. 20. Variation of u/V as a function of z/a along the symmetric axis of a cylinder for the case when $Re = 0.2$, $a/b = 2/3$, $a/R = 0$, $\eta_0 = 100$ poise, $\lambda = 132.2$ s, and $n = 0.69$. Discrete symbols, experimental data of Maalouf and Sigli [28]; solid curve, result predicted by the present analysis.

The variations of X as a function of n at various a/b for two different Re are presented in Fig. 18. Note that if $n = 1$, the fluid is Newtonian. Fig. 18 suggests that X increases with an increase in n. This is expected since the smaller the n the more significant the shear-thinning nature of the fluid. For the case $Re = 0.1$, X increases 389, 371, and 357% as n varies from 0.4 to 1 for a/b equal to 2/3, 1, and 4/3, respectively, and for the case $Re = 40$, X increases 357, 317, and 285% as n varies from 0.4 to 1 for a/b equal to 2/3, 1, and 4/3, respectively. These imply that the shape effect of a particle can be easily distinguished by varying n, and the effect of n on X at a low Re is more important than that at a high Re.

As pointed out by Clift et al. [4], flow separation in the wake behind a particle can be checked by a change in the sign of the vorticity contour on particle surface and first occurs at the rear stagnant point. The critical Reynolds number, Re_c, the Re at the onset of flow separation, is defined by

$$Re_c = \frac{2\rho a V_c}{\eta_0}, \tag{13}$$

where V_c is the velocity at the onset of flow separation. Fig. 19 shows the variation of Re_c as a function of n for various types of particle at $a/R = 0.7$. It should be pointed out that because judging Re_c based on the above-mentioned criterion is not an easy task, only approximate results are obtained. The scattering of the data presented in Fig. 19 reflects this. In general, Re_c increases roughly linearly with the increase in n for the types of particle and the range of n examined.

The applicability of the present model is examined by fitting it to the experimental data of Maalouf and Sigli [28], where the effect of the shape of a body fixed on the axis of a cylinder filled with a viscoelasticity fluid on the fluid velocity around the body is investigated. For the case of a shear-thinning fluid, a power law relation

$$\eta = K|\dot{\gamma}|^{m-1} \tag{14}$$

is used, where K and m are constant. The rheological properties of the shear-thinning fluids used by them are $K = 22$ g/(cm^2 s) and $m = 0.69$. The corresponding parameters in the present Carreau model are $\eta_0 = 100$ poise, $\lambda = 132.2$ s, and $n = 0.69$. The experimental data of Maalouf and Sigli which describe the variation of the downstream and the upstream velocity distribution along the axis of the cylinder are presented in Fig. 20. The results based on the present analysis are shown in this figure. As can be seen from Fig. 20, the performance of the present model is satisfactory.

In an experimental study of the wall effect on a sphere of radius a moving along the axis of a cylinder of radius R filled with a viscoelastic fluid, Chhabra et al. [6] arrived at the correlation below for the wall factor $f = V/V_\infty$, V_∞ being the velocity of a sphere moving in an infinite medium:

$$f = 1 - 1.3(a/R)^{0.94} Cu^{-0.077}. \tag{15}$$

Fig. 21 shows the result based on this relation and that calculated by the present method. As can be seen from this figure, the agreement between the two is satisfactory; the maximum

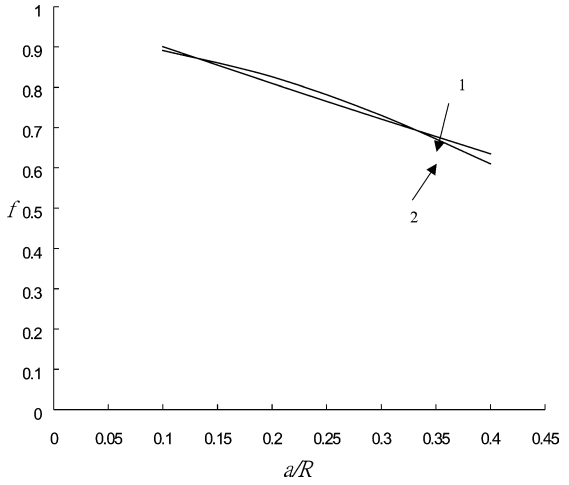

Fig. 21. Variation of f as a function of a/R for the case when $Re = 0.96$, $a/b = 1$, $Cu = 200$, $\eta_0 = 300$ poise, $\lambda = 20$ s, and $n = 0.5$. Curve 1, experimental data of Chhabra et al. [6]; 2, result predicted by the present analysis.

difference between the two in the range of a/R examined is less than 4%.

4. Conclusion

In summary, the boundary effect on a rigid, nonspherical entity in a Carreau fluid is examined by considering the movement of a spheroidal particle along the axis of a cylinder. Numerical simulations are conducted for Reynolds numbers in the range $(0.1, 40)$, Carreau numbers in the range $(0, 1)$, and the parameter (semiaxis in radial direction/radius of cylinder) in the range $(0, 0.8)$. We show that for a prolate, the ratio (drag correction factor of spheroid in shearing–thinning fluid/factor in a Newtonian fluid), has a maximum as the ratio (semiaxis in radial direction/radius of cylinder) varies, but this is not observed for an oblate. For a fixed semiaxis in the radial direction, the magnitude of the drag coefficient, from the smallest to the largest, follows the order prolate $>$ sphere $>$ oblate, which is also true for the case of a Newtonian fluid. The presence of a cylinder wall has the effect of depressing the formation of the wakes in the real part of a particle. If the wall effect is unimportant, the shear-thinning nature of the fluid has the effect of reducing its convective motion, which is disadvantageous to the formation of wakes; the reverse is true if the wall effect is important. This phenomenon is more obvious for an oblate than for a prolate. The influence of the shape of a particle on the drag force it experiences can be decreased by either increasing the shear-thinning effect of the fluid or increasing the Reynolds number. For both prolate and oblate, the closer the fluid to a Newtonian fluid the larger the Reynolds number at the onset of flow separation, and their relation is roughly linear.

Acknowledgment

This work is supported by the National Science Council of the Republic of China.

References

[1] H. Brenner, Chem. Eng. Commun. 148 (1996) 487–562.
[2] S. Blaser, Chem. Eng. Sci. 57 (2002) 515–526.
[3] R.P. Chhabra, Powder Technol. 85 (1995) 83–90.
[4] R. Clift, J. Grace, M.E. Weber, Bubbles, Drops and Particles, Academic Press, New York, 1978.
[5] R.P. Chhabra, Bubbles, Drops, and Particles in Non-Newtonian Fluids, CRC Press, Boca Raton, FL, 1993.
[6] R.P. Chhabra, C. Tiu, P.H.T. Uhlherr, Can. J. Chem. Eng. 59 (1981) 771–775.
[7] P.Y. Huang, J. Feng, D.D. Joseph, J. Fluid Mech. 271 (1994) 1–16.
[8] Q. Xu, E.E. Michaelides, Int. J. Numer. Methods Fluids 22 (1996) 1075–1087.
[9] A. Tripathi, R.P. Chhabra, T. Sundararajan, Ind. Eng. Chem. Res. 33 (1994) 403–410.
[10] R.P. Chhabra, P.H.T. Uhlherr, Can. J. Chem. Eng. 58 (1980) 124–128.
[11] Y.J. Liu, D.D. Joseph, J. Fluid Mech. 255 (1993) 255–595.
[12] V. Navez, K. Walters, J. Non-Newtonian Fluid Mech. 67 (1996) 325–334.
[13] B. Mena, O. Manero, L.G. Leal, J. Non-Newtonian Fluid Mech. 26 (1987) 247–275.
[14] D. Rodrigue, D. De Kee, C.F. Chan Man Fong, Chem. Eng. Commun. 154 (1996) 203–215.
[15] N. Shahcheraghi, H.A. Dwyer, J. Heat Transfer 120 (1998) 985–990.
[16] A. Tripathi, R.P. Chhabra, AIChE J. 41 (1995) 728–731.
[17] R.M. Turian, Am. Inst. Chem. Eng. J. 13 (1967) 999–1006.
[18] P.H.T. Uhlherr, T.N. Le, C. Tiu, Can. J. Chem. Eng. 54 (1976) 497–502.
[19] K.A. Missirlis, D. Assimacopoulos, E. Mitsoulis, R.P. Chhabra, J. Non-Newtonian Fluid Mech. 96 (2001) 459–471.
[20] K. Ceylan, S. Herdem, T. Abbasov, Powder Technol. 103 (1999) 286–291.
[21] I. Machač, B. Šiška, L. Machačcvá, Chem. Eng. Proc. 39 (2000) 365–369.
[22] G. McKinley, Transport Processes in Bubbles, Drops and Particles, second ed., Taylor & Francis, New York, 2002.
[23] R.B. Bird, R.C. Armstrong, O. Hassager, Dynamics of Polymeric Liquids, Wiley, New York, 1977.
[24] H.A. Barnes, J.F. Hutton, K. Walters, An Introduction to Rheology, Elsevier, New York, 1989.
[25] J. Ferguson, Z. Kemblowski, Applied Fluid Rheology, Elsevier, New York, 1991.
[26] R.B. Bird, W.E. Stewart, E.N. Lightfoot, Transport Phenomena, Wiley, New York, 1960.
[27] J. Happel, H. Brenner, Low Reynolds Number Hydrodynamics, Academic Press, New York, 1983.
[28] A. Maalouf, D. Sigli, Rheol. Acta 23 (1984) 497–507.